






Twin spotlight beam generation in quadratic crystals

Raphaël Jauberteau ^{1,2✉}, Sahar Wehbi¹, Tigran Mansuryan¹, Alessandro Tonello¹, Fabio Baronio ², Katarzyna Krupa³, Benjamin Wetzel ¹, Stefan Wabnitz ⁴ & Vincent Couderc ¹

Optical rogue waves have been extensively studied in the past two decades. However, observations of multidimensional extreme wave events remain surprisingly scarce. In this work we present the experimental demonstration of the spontaneous generation of spatially localized two-dimensional beams in a quadratic nonlinear crystal, which are composed by twin components at the fundamental and the second-harmonic frequencies. These localized spots of light emerge from a wide background beam, and eventually disappear as the laser beam intensity is progressively increased.

¹ Université de Limoges, XLIM, UMR CNRS 7252, 123 Avenue A. Thomas, 87060 Limoges, France. ² Dipartimento di Ingegneria dell'Informazione, Università di Brescia, via Branze 38, 25123 Brescia, Italy. ³ Institute of Physical Chemistry, Polish Academy of Sciences, Warsaw, Poland. ⁴ DIET, Sapienza University of Rome, Via Eudossiana 18, 00184 Rome, Italy. ✉email: raphael.jauberteau@gmail.com

Solitons are self-sustained nonlinear waves, and the abundance of their observations in many different nonlinear media is proof of their universal nature^{1,2}. In fiber optics, ultrashort pulses usually spread in time as a result of group velocity dispersion (GVD). On the other hand, temporal solitons are special pulses which self-preserve their temporal envelope, when GVD is stably compensated by fiber nonlinearity. Solitons in optical fibers are exact solutions of the well-known 1-dimensional (1D) nonlinear Schrödinger equation (NLSE)^{3–5}. Continuous waves or long pulse envelopes instead can have a completely different fate: they can be unstable against temporal perturbations and eventually break up in a train of short pulses. Although the early stages of this process, which is known as modulational instability, can be described by a simple linear stability analysis, the nonlinear stage of the evolution of modulation instability can also be described in terms of analytical solutions of the NLSE. Among these nonlinear modulation waves, we may cite the so-called Akhmediev breathers⁶, Peregrine solitons⁷, and Kuznetsov-Ma breathers^{8,9}. All of those nonlinear waves exhibit localization both in the temporal and in the longitudinal (or propagation) coordinates. Specifically, Peregrine solitons are often referred to as an example of waves that “appear from nowhere, and disappear without a trace”¹⁰. All of these waves have been clearly observed in optical fiber experiments, although most of their theory was first developed in the context of hydrodynamics^{11–13}. In spite of being fully deterministic solutions of the 1D-NLSE, nonlinear modulation waves have been proposed as a fundamental model for rogue waves, which represent statistical extreme events in many different physical settings, such as oceanography. The randomness of the initial conditions for wave propagation associates rogue waves to the appearance of rare events, whose presence can be detected by long-tails in the probability distribution of, e.g., the wave height¹⁴.

The origin of the success of the 1D-NLSE model is associated with its generality for describing wave propagation in weakly (cubic) nonlinear and dispersive media, as well as its full integrability by the inverse scattering method. Notably, deterministic rogue waves have been also predicted in media with quadratic nonlinearity. In this case, the three-wave mixing equations apply, which is another example of a fully integrable nonlinear wave model^{15,16}. Incidentally, under the approximation known as cascading, the three-wave mixing equations can also be reduced to the 1D-NLSE.

If one replaces the temporal coordinate with a transverse spatial coordinate, the 1D-NLSE equation describes beam propagation when diffraction (analogous to dispersion) is affecting the local beam size (analogous to the pulse temporal envelope). The analogy is an immediate draw since the transverse spatial domain is inherently bidimensional, while the time domain is naturally described by a single dimension. A good approximation for a one-dimensional “flat” transverse spatial dimension is provided by the case of a slab waveguide (or possibly a very elliptical beam): spatial extreme waves have been predicted to appear in 1D quadratic media^{17–19}. A further extension of the NLSE model could be considered for arrays of waveguides or for multimode propagation in a waveguide: in both cases, multimodality can be seen as a synthetic transverse dimension. Indeed, soliton solutions exist both in arrays of waveguides and in multimode fibers^{20,21}.

When the full bidimensional nature of the transverse spatial domain is considered, the beam propagation problem is far more complex, and many dynamical systems are no longer integrable. Nevertheless, both “solitons” (under their less demanding definition of nonlinear self-preserving waves) and modulation instabilities have been reported for 2D systems^{22–26}. When the interacting optical waves have different linear group velocities, in

the presence of diffraction and nonlinearity, the nonlinear wave models increase their complexity. In nonlinear media with dominant quadratic susceptibility and in the presence of crystal anisotropy, spatial 2D solitons are conditionally stable solutions. This is the case of walking solitons²⁷, with their related beam instabilities^{28,29}.

The existence of extreme waves in 2D wave systems is still an open question: this is new territory yet largely to be explored. The first endeavor in this research direction was the numerical prediction of rogue waves, as reported in ref. ³⁰. Spatial 2D rogue waves and caustics generated by nonlinear instabilities have been studied by means of a statistical approach in³¹. Some mathematical models also predict the existence of 2D deterministic rogue waves: for example, the three-wave mixing model which describes the nonlinear coupling between a fundamental frequency (FF) wave and its second harmonic (SH). Remarkably, under some approximations^{32,33} one obtains an integrable model, in the frame of which the existence of extreme waves has been recently predicted³². Another important consideration is that, when dealing with the propagation of nearly plane waves or relatively wide beams, that is, of intrinsically 2D waves, the observation of spatial modulation instability in quadratic media has been reported^{34–36}. However, when taking into account the presence of the temporal dimension, then the analysis of modulation instabilities should be extended to fully 3D waves. In analogy with the 1D case¹¹, it is then natural to speculate whether in a 2D crystal with quadratic nonlinearity or even in 3D quadratic systems (when time is also considered), the decay (or the instabilities) of spatially localized solutions which is observed when, e.g., the input power is varied, can be interpreted as a signature of the underlying existence of rogue waves.

The present work demonstrates we believe, for the first time, in the generation of extreme light beams in anisotropic crystals with quadratic nonlinearity. Specifically, we report the experimental observation of a deterministic 2D spatial twin spotlight beam (TSB), which appears from nowhere and disappears without a trace as the input laser power is progressively increased. By twin beam, we mean a beam composed of two frequency components, one at the FF and one at the SH frequency.

Results and discussion

Our experimental analysis was carried out with a sample of Potassium Titanyl Phosphate, a nonlinear crystal with quadratic susceptibility, commonly known as KTP. The crystal, 30 mm long, was cut to maximize the efficiency of second harmonic generation (SHG) by exploiting its anisotropic nature at room temperature. The nonlinear process is known as type-II SHG, as it involves the nonlinear coupling of the two polarization components of the input FF beam, propagating along the ordinary and extraordinary axis of the crystal, and the SH wave, which is polarized along the extraordinary axis. Light propagation in anisotropic crystals (in the specific case, the KTP is an orthorhombic biaxial crystal) is quite peculiar, since the wavevector (the vector normal to the wave fronts) does not align, in general, with the direction of the energy flow (the Poynting vector). Fig. 1 gives a visual interpretation of the nonlinear frequency conversion process. The input optical beam is linearly polarized: the electric field forms an angle α with the horizontal reference axis. The white arrow represents the wavevector of the FF, while the Poynting vectors are indicated in red for the FF and in green for the SH. The Poynting vector of the FF extraordinary wave (e) has a spatial walk-off angle ρ_1 with the horizontal axis. Similarly, the Poynting vector of the SH wave (e) has a spatial walk-off angle ρ_2 . Figure 1 also shows the orientation of the KTP crystallographic axes, X, Y, and Z, as well as the two relevant angles θ and φ with

respect to the propagation reference frame, which are used in order to control the phase matching for type-II SHG.

Experiments have been carried out close to the values $\theta = 90^\circ$, $\varphi = 23.5^\circ$ at the phase matching of type-II SHG. Small angle tilts out of these reference values are a common way to introduce a controlled phase mismatch. In our experiments, we noticed the presence of a spatial asymmetry among the three waves, which we may explain by the presence of an additional walk-off of the (pseudo) ordinary axis, which we indicated by ρ_0 . As it is well-known, these walk-off angles and the consequent beam splitting induce limits to the effective nonlinear interaction length along the propagation direction.

In order to demonstrate the generation of a spatial two-dimensional TSB, let us consider first a series of experimental results obtained with a polarization orientation angle $\alpha = 47^\circ$: such a choice imposes a power unbalance in the FF between the ordinary and the extraordinary axis. Figure 2 summarizes the experimentally obtained spatial beam shapes of the FF and the SH for different input intensities. When the intensity is relatively low, we observed only weak conversion into the SH in absence of any change of shape in the FF (see Fig. 2a for FF and Fig. 2e for SH).

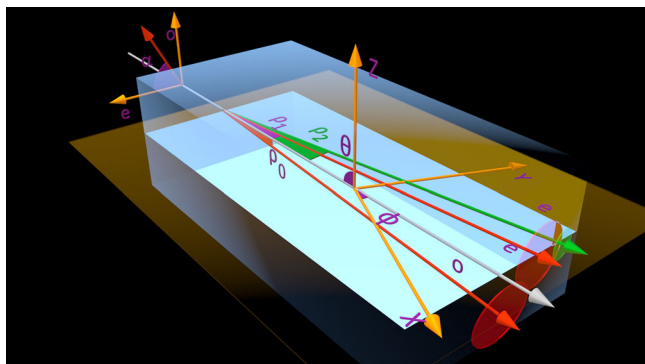


Fig. 1 Graphical illustration of beam propagation in potassium titanyl phosphate (KTP) crystals. The fundamental frequency (FF) ordinary (o), FF extraordinary (e), and the second harmonic (SH) beams have different walk-off angles, ρ_0 , ρ_1 , and ρ_2 , respectively. The orientation of the reference frame with respect to the crystallographic axes X, Y, and Z is identified by the angles θ and φ . The orientation of the input linear polarization of the light beam is measured by the angle α .

When we increased the input FF beam intensity up to 0.07 GW/cm^2 , we observed the formation of a narrow-coupled FF-SH beam trapped at the intersection of the two diverging beams at the FF. Such a self-focused beam, or TSB, has a diameter of $\sim 40 \mu\text{m}$, that is about ten times smaller than the diameter of the input FF beam. The TSB, which results from a strong reshaping of the input FF beam, has the main features of a spatial soliton surrounded by radiation:²⁷ it involves both spectral components at the FF and the SH, as shown in Fig. 2b, c, f, g. The maximum peak intensity of the TSB, which is 2.7 times higher than that of the encircling background, is reached for an input FF intensity of 0.64 GW/cm^2 (see Fig. 2c).

Now, surprisingly, we observed that by increasing further the input FF intensity, the TSB suddenly vanished (see Fig. 2d): its existence is thus confined to a limited range of input intensity values. At relatively high intensities, the smooth FF background beam recovers a spatial profile, which is nearly as wide as that observed at low intensities, except for the presence of minor residual distortions. To summarize, upon an increase of the input laser intensity, the TSB is first formed, then it grows up to an intensity elevation, which is nearly three times that of the local background, and then it disappears without leaving a visible trace. The observed TSB dynamics is thus very different from that of spatial solitons, which tend to persist and can even be strengthened upon increasing input FF intensity. It is important to notice that as the FF component of the TSB grows up, its shape is replicated at the SH, with high contrast from the associated background. However, the beam dynamics at the FF and the SH are very different at very high intensities (cf. Fig. 2d, h).

As can be seen, although the high-energy located spot at the FF nearly disappears, beam-breaking occurs at the SH. Specifically, for input intensities of 9.3 GW/cm^2 , the SH breaks up into a speckled beam (Fig. 2h and Fig. SM4 in Supplementary Note 3). The process of beam-breaking at the SH has been studied in detail in a related study³⁷.

Figure 3 collects many different transverse beam sections at the FF vs. the input FF intensity: panel 3(a) clearly shows the appearance and the vanishing of the TSB. Whereas panel 3(b) clarifies the quantitative dependency of the TSB to background intensity contrast vs. the input intensity.

We observed that the TSB generation is influenced, similarly to quadratic spatial solitons, by the power unbalance between the two polarization components of the beam at the FF, as

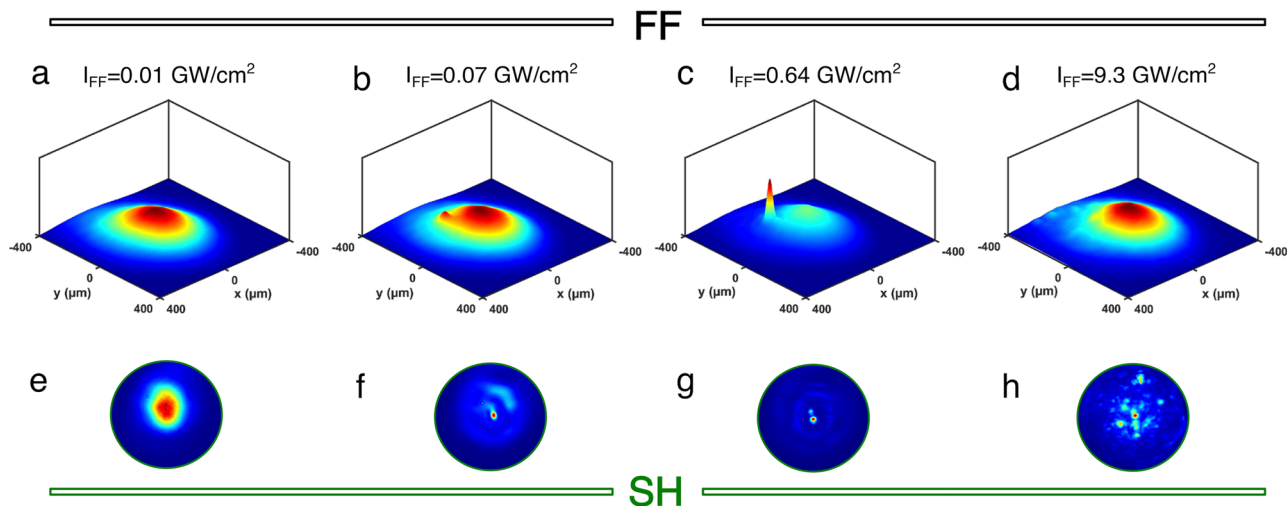


Fig. 2 Output twin spotlight beam (TSB) profiles when increasing the input beam intensity I_{FF} . a–d Refer to the fundamental frequency (FF). e–h Show the corresponding second harmonic (SH) intensity profile. Color gradient goes from blue (the lowest light peak intensity) to red (the highest light peak intensity).

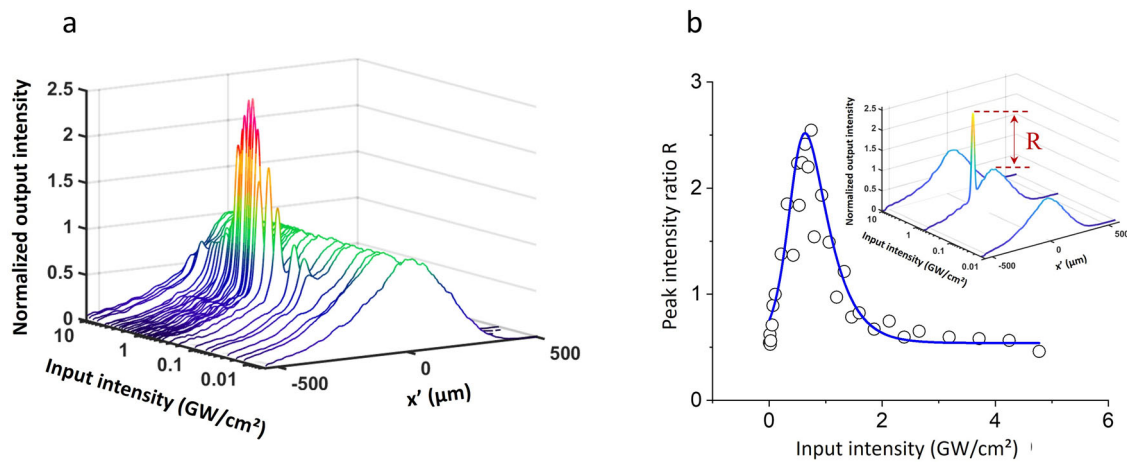


Fig. 3 Fundamental frequency (FF) transverse beam sections at the crystal output. **a** Twin spotlight beam (TSB) sections of the FF component of the TSB vs. input FF intensity; **b** peak intensity measuring the intensity elevation of the FF component of the TSB from the local background vs. input FF intensity. R is the peak intensity ratio between the top of the TSB and the encircling background.

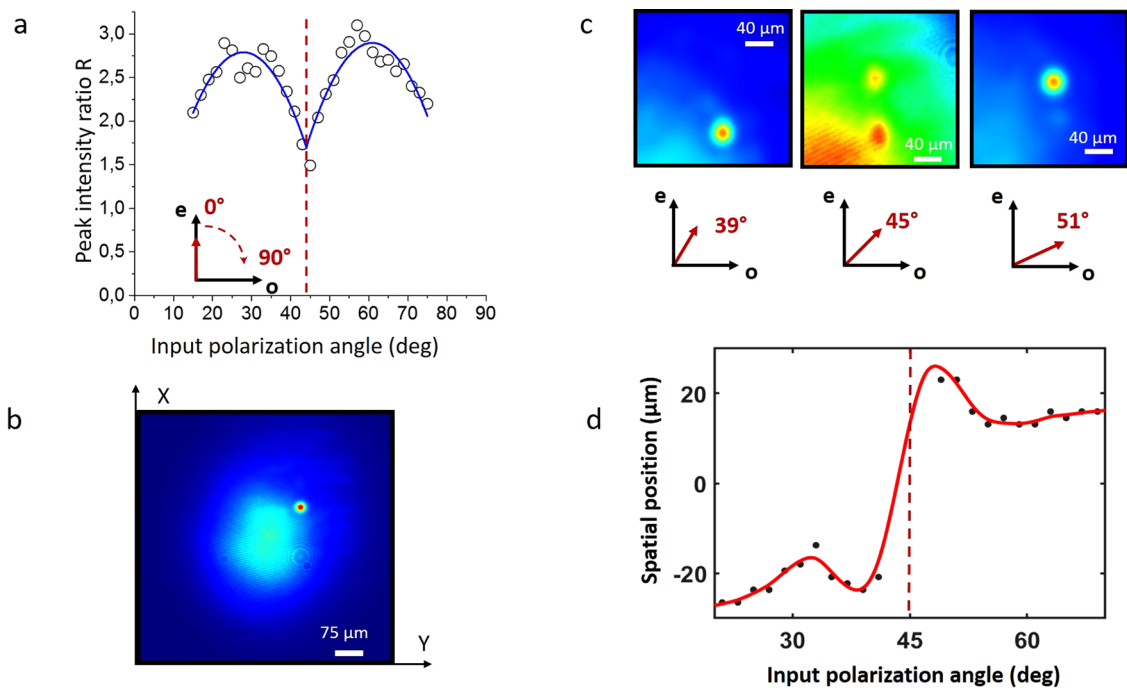


Fig. 4 Experimental results on the efficiency of the 2D spatial twin spotlight beam (TSB) trapping and associated spatial switching. **a** Peak intensity ratio between the TSB and the input beam; **b** Example of TSB generation for an input polarization orientation angle $\alpha = 60^\circ$; **c** Example of TSB spatial switching for three different input polarization angles; **d** Spatial position of the TSB vs. the input polarization angle α (input beam intensity $I_{FF} = 0.64 \text{ GW/cm}^2$).

determined by the polarization orientation angle α . Since the beams carried by each of the two polarization components have slightly different propagation directions (owing to spatial walk-off), by modifying the polarization angle α , the spatial position of the TSB can abruptly hop from one output spatial position to another one. Although the TSB is systematically obtained for all angles from $\alpha = 10^\circ$ to $\alpha = 80^\circ$ for a fixed FF intensity, the elevation of the FF component of the TSB from the surrounding background and its spatial position varies: maximum TSB intensity is reached for two symmetric polarization orientation angles, close to either $\alpha = 30^\circ$ and $\alpha = 60^\circ$ (Fig. 4a): the corresponding spatial shape is given in panel (4b). When the input polarization angle was set to $\alpha = 45^\circ$ (i.e., equal input FF intensities in both polarization axes), we observed the presence of two competing TSBs (Fig. 4c, d). Panel (c) shows an example of

spatial switching of the TSB position for three particular values of α ; while panel (d) illustrates the sharp nonlinear transition of the spatial TSB position for a set of values of the orientation angle α . Note that analogous dynamics were earlier reported for spatial solitons^{38,39}: the sharp dependence of the output beam position on the input state of polarization could find possible applications to ultrafast all-optical switching, as polarization comparator²⁴, or even, by extension, as an optical implementation of an activation function for an artificial neuron.

Additionally, in the large positive phase mismatch regime, we also observed the presence of multiple TSBs (see Fig. SM1 in supplementary note 1).

In our experimental analysis, we found that the generation of the TSB not only involves the spatial domain, as it can be detected by a slow-time response camera but also has a direct influence on

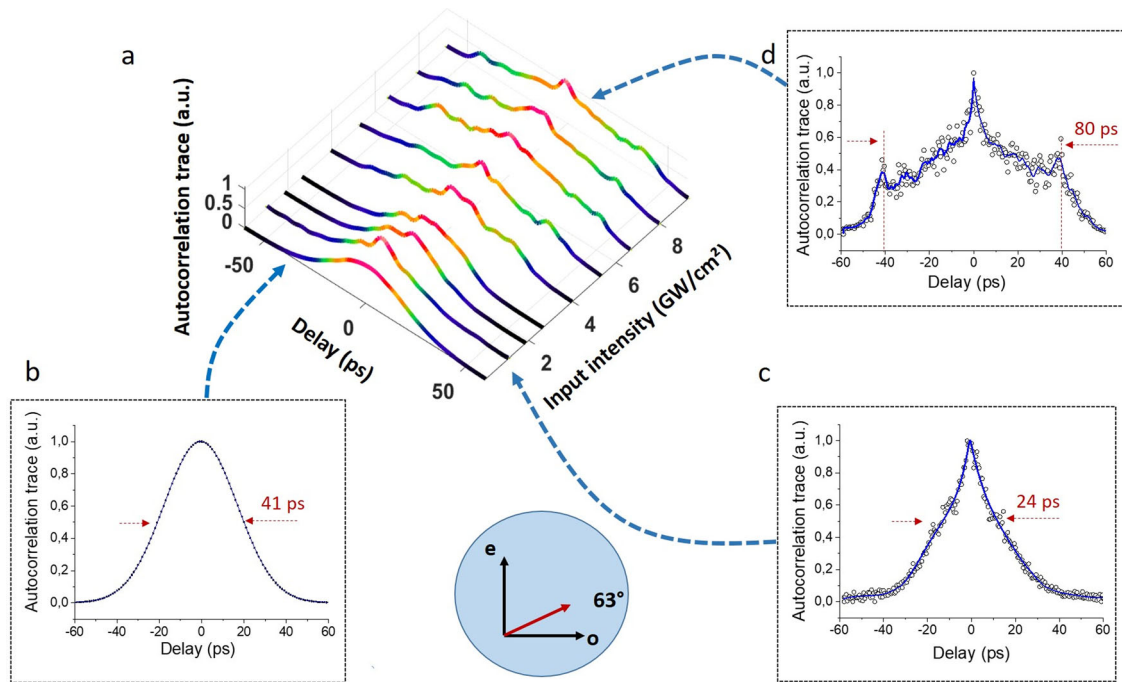


Fig. 5 Time domain analysis of pulses from the output fundamental frequency (FF) component of the twin spotlight beam (TSB). **a** Autocorrelation traces at different input intensities for perfect phase matching. Details of the traces: **b** Autocorrelation of the input laser pulse; **c** Autocorrelation at 1 GW/cm^2 ; **d** Autocorrelation taken at high FF intensities, such that the TSB has nearly vanished. The circular inset illustrates the orientation of the linear polarization state of the input beam.

the temporal shape of the FF component of the TSB. For analyzing temporal reshaping effects in detail, we measured the temporal autocorrelation within the TSB area, and we varied the input FF intensity (cf. Fig. 5a) as well as the FF-SH phase mismatch. At low input intensities, the temporal autocorrelation trace has a Gaussian shape with a 41 ps temporal width (compatible with a pulse duration of 29 ps FWHMI), see Fig. 5b. However, once the TSB is formed, the shape of the autocorrelation trace takes a nearly triangular profile of 24 ps (FWHMI), see Fig. 5c. At even higher input powers, where the TSB is close to its vanishing, the temporal autocorrelation trace exhibits several peaks, which can be associated with a temporal break-up of the underlying pulse, see Fig. 5d. Interestingly, different behavior is observed for positive and negative values of the phase mismatch (cf. Figs. SM2, SM3 in the supplementary note 2). Indeed, it is known that temporal modulational instability may occur for both positive and negative values of the phase mismatch in quadratic crystals. However, asymmetric evolutions (i.e., different gain profiles) of the sidebands are obtained when changing the sign of phase mismatch⁴⁰. Note that spectral sideband generation at the FF and the SH have also been experimentally reported in ref. ³⁶ for similar pulse durations.

We would like to underline that the nature of the observed extreme TSB is fully deterministic and reproducible. We confirmed its deterministic nature by numerically solving the nonlinear coupled equations involving the three interacting waves, i.e., the two FF beams and the SH wave. In the model, we included all relevant effects, namely diffraction and quadratic susceptibility. We limited our numerical analysis to the case of a simple spatial interaction of the three waves, thus neglecting the temporal dimension. Moreover, our analysis was limited to walk-off angles corresponding to the two extraordinary waves, and we set to zero, for simplicity, the FF ordinary beam angle ρ_0 . The input beam had a Gaussian profile with a $400\text{-}\mu\text{m}$ diameter, and we superimposed to it a weak bump, whose center had an offset of $200\text{ }\mu\text{m}$ in one of the spatial coordinates, which was used as a seed.

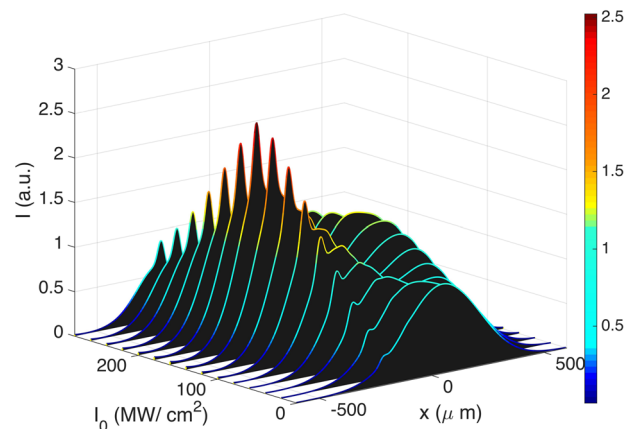


Fig. 6 Numerically simulated sections of the fundamental frequency (FF) component of the twin spotlight beam (TSB) vs. the input intensity I_0 .

The images have been collected after propagation of 30 mm. The color bar relates to the light peak intensity (normalized with the encircling background).

In Fig. 6, we show a collection of numerically computed output FF components of the TSB for different input intensities. As can be seen by comparing Fig. 6 with Fig. 3a, numerical simulations agree well with experimental results. In particular, the intensity of the FF component of the TSB grows up to an elevation of about 2.5 times the background intensity. Then the TSB progressively disappears when the input FF beam intensity grows larger. A numerical study of the FF beam shape at different positions along the crystal and at fixed input intensity is also given in supplementary note 4 (Fig. SM5).

In conclusion, we demonstrated that a coupled FF and SH 2D spotlight beam can appear and disappear at the output of a quadratic crystal in the presence of a monotonic increase of the input FF beam intensity. Such a beam bears a strong resemblance

to fully localized waves such as the Peregrine temporal soliton of the 1D-NLSE, which also appears and disappears as the input power grows larger, thanks to the equivalence between varying power or propagation length. However, the localized wave that we have unveiled here emerges in the frame of a genuine 2D nonlinear wave coupling process. Besides the resemblance with other types of extreme waves, the full nature of the extreme or rogue wave described in the present work appears to involve a coupling between its spatial and temporal dimensions. Additionally, we showed how the spatial position of the TSB can abruptly switch upon a relatively small change in the linear polarization angle of the input FF beam. Although phase mismatched SHG seems to be the dominant nonlinear process in the early stage of the TSB generation, the observed temporal wave breaking at the FF could provide the mechanism which is responsible for its disappearance at high intensities.

Methods

Experiments. We used a laser source at 1064 nm, delivering pulses of 30 ps with pulse energies up to several tens GW/cm² and a repetition rate of 10 Hz. The linearly polarized beam was collimated in the nonlinear crystal (beam diameter of 400 μm at 1/e² in intensity) by means of a convergent lens ($f=10$ cm, the Fresnel length associated to the beam is more than six times longer than the crystal length) and a half-wave plate, which allows for setting the polarization orientation of the input beam. An output convergent lens ($f=3.5$ cm) was used to obtain a magnified image of the output end face of the crystal on a CCD camera. An autocorrelator was used to obtain the temporal evolution of the output FF beam. We used a type-II KTP crystal cut for second harmonic generation at 1064 nm. The spatial walk-off between the two FF beams and the SH is 3.48 mrad and 4.88 mrad, respectively. The phase matching conditions were controlled through crystal orientation in horizontal or vertical dimensions. Additional experimental results are discussed in the supplementary material notes 1 to 3, and the reader can also find further information about the experimental setup in ref. ⁴¹ Temporal autocorrelations were obtained by selecting the TSB with a diaphragm and then by measuring the autocorrelation at the FF.

Numerical simulations. We numerically solved the three-wave equations by considering the presence of diffraction, the spatial walk-off between the FF and SH, and the quadratic nonlinear response of the KTP at the relevant angles close to phase matching. The numerical integration scheme was based on a standard Runge-Kutta method. Details on the three-wave equations and simulation parameters can be found in supplementary note 4.

Data availability

The data supporting the findings of this research are available upon request from the corresponding author.

Code availability

The code supporting the simulation plots inside our paper are available upon request from the corresponding author.

Received: 15 November 2021; Accepted: 19 July 2022;

Published online: 04 August 2022

References

1. Scott Russell, J. "Report on waves." In *14th Meeting of the British Association for the Advancement of Science* (1844).
2. Remoissenet, M. *Waves Called Solitons. Concepts and Experiments* (Springer, 1999).
3. Zakharov, E. & Shabat, A. B. Exact theory of two-dimensional self-focusing and one-dimensional self-modulation of wave in nonlinear media. *J. Exp. Theor. Phys.* **34**, 62 (1972).
4. Hasegawa, A. & Tappert, F. Transmission of stationary nonlinear optical pulses in dispersive dielectric fibers I. Anomalous dispersion. *Appl. Phys. Lett.* **23**, 142 (1973).
5. Mollenauer, L. F., Stolen, R. H. & Gordon, J. P. Experimental observation of picosecond pulse narrowing and solitons in optical fibers. *Phys. Rev. Lett.* **45**, 1095 (1980).
6. Akhmediev, N. & Korreev, V. I. Modulation instability and periodic solutions of the nonlinear Schrödinger equation. *Theor. Math. Phys.* **69**, 1089–1093 (1986).
7. Peregrine, D. H. Water waves, nonlinear Schrödinger equation and their solutions. *Aust. Math. Soc. Ser. B, Appl. Math.* **25**, 16 (1983).
8. Kuznetsov, E. A. Soliton in a parametrically unstable plasma. *Sov. Phys. Dokl.* **22**, 507–508 (1977).
9. Ma, Y. C. The perturbed plane-wave solutions of the cubic Schrödinger equation. *Stud. Appl. Math.* **60**, 43–58 (1979).
10. Akhmediev, N., Soto-Crespo, J. M. & Ankiewicz, A. Extreme waves that appear from nowhere: on the nature of rogue waves. *Phys. Lett. A* **373**, 2137–2145 (2009).
11. Kibler, B. et al. The peregrine soliton in nonlinear fiber optics. *Nat. Phys.* **6**, 790 (2010).
12. Dudley, J. M., Genty, G., Dias, F., Kibler, B. & Akhmediev, N. Modulation instability, Akhmediev breathers and continuous wave supercontinuum generation. *Opt. Express* **17**, 21497–21508 (2009).
13. Kibler, B. et al. Observation of Kuznetsov-Ma soliton dynamics in optical fibre. *Sci. Rep.* **2**, 463 (2012).
14. Onorato, M., Residori, S., Bortolozzo, U., Montina, A. & Arcchi, F. T. Rogue waves and their generating mechanisms in different physical contexts. *Phys. Rep.* **528**, 47–89 (2013).
15. Baronio, F., Conforti, M., Degasperis, A. & Lombardo, S. Rogue waves emerging from the resonant interaction of three waves. *Phys. Rev. Lett.* **111**, 114101 (2013).
16. Stegeman, G. I., Sheik-Bahae, M., Van Stryland, E. & Assanto, G. Large nonlinear phase shifts in second-order nonlinear-optical processes. *Opt. Lett.* **18**, 13–15 (1993).
17. Baronio, F. Akhmediev breathers and Peregrine solitary waves in a quadratic medium. *Opt. Lett.* **42**, 1756–1759 (2017).
18. Baronio, F., Chen, S. & Mihalache, D. Two-color walking Peregrine solitary waves. *Opt. Lett.* **42**, 3514–351 (2017).
19. Schiek, R. & Baronio, F. Spatial Akhmediev breathers and modulation instability growth-decay cycles in a quadratic optical medium. *Phys. Rev. Res.* **1**, 032036 (2019).
20. Aceves, A. B., De Angelis, C., Rubenchik, A. M. & Turitsyn, S. K. Multidimensional solitons in fiber arrays. *Opt. Lett.* **19**, 329–331 (1994).
21. Crosignani, B. & Porto, P. D. Soliton propagation in multimode optical fibers. *Opt. Lett.* **6**, 329–330 (1981).
22. Barthelemy, A., Maneuf, S. & Froehly, C. Propagation soliton et autoconfinement de faisceaux laser par non linearité optique de kerr. *Opt. Commun.* **55**, 201 (1985).
23. Torruellas, W. E. et al. Observation of two-dimensional spatial solitary waves in a quadratic medium. *Phys. Rev. Lett.* **74**, 25 (1995).
24. Bourliaguet, B. et al. Observation of quadratic spatial solitons in periodically poled lithium niobate. *Opt. Lett.* **24**, 1410 (1999).
25. Buryak, A. V., Di Trapani, P., Skryabin, D. V. & Trillo, S. Optical solitons due to quadratic nonlinearities: from basic physics to futuristic applications. *Phys. Rep.* **370**, 63–235 (2002). (2002).
26. Trillo, S. & Torruellas, W. (eds) *Spatial Solitons* (Springer, 2001).
27. Mihalache, D., Mazilu, D., Crasovan, L.-C. & Torner, L. Walking solitons in type II second-harmonic generation. *Phys. Rev. E* **56**, R6294 (1997).
28. Buryak, A. V., Kivshar, Y. & Trillo, S. Stability of three-wave parametric solitons in diffractive quadratic media. *Phys. Rev. Lett.* **77**, 5210–5213 (1996).
29. Buryak, A. V. & Kivshar, Y. Multistability of three-wave parametric self-trapping. *Phys. Rev. Lett.* **78**, 3286–3289 (1997).
30. Osborne, A. R., Onorato, M. & Serio, M. The nonlinear dynamics of rogue waves and holes in deep-water gravity wave trains. *Phys. Lett. A* **275**, 386–393 (2000).
31. Safari, A., Fickler, R., Padgett, M. J. & Boyd, R. W. Generation of Caustics and Rogue waves from nonlinear instability. *Phys. Rev. Lett.* **119**, 203901 (2017).
32. Ablowitz, M. J., Biondini, G. & Blair, S. Nonlinear Schrödinger equations with mean terms in nonresonant multidimensional quadratic material. *Phys. Rev. E* **63**, 046605 (2001).
33. Guo, L. et al. Two-dimensional rogue waves on zero background in a Benney-Roskes model. *Phys. Rev. Res.* **2**, 033376 (2020).
34. Delqué, M., Fanjoux, G., Gorza, S.-P. & Haelterman, M. Spontaneous 2D modulation instability in second harmonic generation process. *Opt. Commun.* **284**, 1401–1404 (2011).
35. Trillo, S. et al. Colored conical emission by means of second-harmonic generation. *Opt. Lett.* **27**, 1451–1453 (2002).
36. Krupa, K. et al. Polychromatic filament in quadratic media: spatial and spectral shaping of light in crystals. *Optica* **2**, 1058–1064 (2015).
37. Jauberteau, R. et al. Boosting and taming wave breakup in second harmonic generation. *Fron. Phys.* <https://doi.org/10.3389/fphy.2021.640025> (2021).
38. Torruellas, W. E., Assanto, G. & Lawrence, B. L. All-optical switching by spatial walkoff compensation and solitary-wave locking. *Appl. Phys. Lett.* **68**, 1449–1451 (1996).

39. Leo, G., Assanto, G. & Torruellas, W. E. Bidimensional spatial solitary waves in quadratic nonlinear bulk media. *J. Opt. Soc. Am. B* **14**, 3134–3142 (1997).
40. Trillo, S. & Ferro, P. Modulational instability in second-harmonic generation. *Opt. Lett.* **20**, 438–440 (1995).
41. Krupa, K. et al. Spatial beam self-cleaning in second-harmonic generation. *Sci. Rep.* **10**, 7204 (2020).

Acknowledgements

We are grateful to A.B. Aceves, M. Ferraro, F. Mangini, Y. Sun, S. Trillo, and M. Zitelli for helpful discussions. V.C. acknowledges the financial support provided by the French ANR through the “TRAFIC project: ANR-18-CE080016-01”; the CILAS Company (ArianeGroup) through the shared X-LAS laboratory; the “Région Nouvelle Aquitaine” through the projects F2MH; the National Research Agency under the Investments for the future program with the reference ANR-10-LABX-0074-01 *Sigma-LIM*. R. J and S. W. were supported by the European Research Council (ERC) under the European Union’s Horizon 2020 research and innovation program (No. 740355).

Author contributions

R.J., V.C, S.Wa., and A.T. designed the research. R.J. made the experiments and analyzed the corresponding data on an experimental setup previously conceived by K.K. F.B. made the simulations and analyzed the numerical results with A.T and B.W. S.We, T.M., and V.C. helped in the data collection process. All authors discussed the data analysis and the interpretation. A.T., V.C., S.Wa., B.W., and R.J. prepared the original manuscript draft, reviewed and edited by all the authors. V.C. and S.Wa managed the supervision and the funding acquisition.

Competing interests

The authors declare no competing interests.

Additional information

Supplementary information The online version contains supplementary material available at <https://doi.org/10.1038/s42005-022-00976-2>.

Correspondence and requests for materials should be addressed to Raphaël Jauberteau.

Peer review information *Communications Physics* thanks Alphonse Houwe and the other, anonymous, reviewer(s) for their contribution to the peer review of this work. Peer reviewer reports are available.

Reprints and permission information is available at <http://www.nature.com/reprints>

Publisher’s note Springer Nature remains neutral with regard to jurisdictional claims in published maps and institutional affiliations.



Open Access This article is licensed under a Creative Commons Attribution 4.0 International License, which permits use, sharing, adaptation, distribution and reproduction in any medium or format, as long as you give appropriate credit to the original author(s) and the source, provide a link to the Creative Commons license, and indicate if changes were made. The images or other third party material in this article are included in the article’s Creative Commons license, unless indicated otherwise in a credit line to the material. If material is not included in the article’s Creative Commons license and your intended use is not permitted by statutory regulation or exceeds the permitted use, you will need to obtain permission directly from the copyright holder. To view a copy of this license, visit <http://creativecommons.org/licenses/by/4.0/>.

© The Author(s) 2022